Method for Simultaneous Wing Aerodynamic and Structural Load Prediction

Mark Drela*
Massachusetts Institute of Technology, Cambridge, Massachusetts

A calculation method is presented for the simultaneous solution of aerodynamic and structural loads on arbitrary high-aspect-ratio wings. The wing aerodynamics are modeled using lifting line theory with roll rate, yaw, and yaw rate effects included. The wing structure is modeled as a nonlinear beam with vertical and horizontal displacement and torsional degrees of freedom. Axial compression effects are also incorporated to permit modeling of wings with external bracing struts or wires. The aerodynamic and structural problems together constitute a coupled nonlinear system for the aerodynamic and structural unknowns, which is discretized and solved using a global Newton method. The overall procedure permits computationally economical prediction of the following: 1) aerodynamic and structural loads for a very wide range of operating conditions, 2) induced drag with static wing twist effects included, 3) lateral and longitudinal wing static stability derivatives and roll-yaw coupling forces incorporating wing deflections, 4) static divergence and aileron reversal speeds, and 5) buckling loads for externally braced wings. Examples are drawn from the wing design of the *Daedalus* human powered aircraft.

Nomenclature

Coordinates and Dimensions

b	=	wingspan
c	=	local wing chord
j, J	=	spanwise node index and maximum index
s_w	=	s location of strut or wire attach point
$(x/c)_{sc}$	=	chordwise shear center location
x, s, n	=	local coordinates fixed to wing section
x, y, z	=	Cartesian coordinates fixed to aircraft
θ	=	spanwise Glauert coordinate
ϑ	=	angle of external bracing wire

Structural Parameters

EA_w	=	tensile stiffness of external strut or wire
EI_{in}	=	in-plane bending stiffness
EI_{nn}	=	x deflection bending stiffness
EI_{out}	=	out-of-plane bending stiffness
EI_{xn}	=	x,n deflection bending cross stiffness
EI_{xx}	=	n deflection bending stiffness
F_f, F_w	=	point load due to fuselage, external bracing
GJ	=	torsional stiffness

Local Structural Solution Variables

M_x, M_n	=	x,n bending moments
P	=	axial tension resultant force
S_x, S_n	=	x,n shear resultant forces
T	=	torsion moment
t	=	torsional twist angle
u, w	=	x,z deflections
φ, ϑ	=	x,z deflection angles

Global Variables and Operating Parameters

A_n	=	bound circulation Fourier coefficients
$\beta, \dot{\beta}, \ddot{\beta}$	=	yaw angle, yaw rate, yaw acceleration
$\phi, \dot{\phi}, \ddot{\phi}$	=	roll angle, roll rate, roll acceleration

Aerodynamic Quantities

a_o	=	two-dimensional airfoil lift-curve slope
c_d, c_l, c_m	=	local profile drag, lift, and pitching moment coefficients
$\mathfrak{L}, \mathfrak{M}, \mathfrak{N}$	=	total lift, rolling moment, yawing moment
V, V_∞	=	local and centerline air velocity
α, α_∞	=	local and freestream angle of attack
α_i	=	induced angle of attack
Γ	=	bound circulation
ρ	=	air density

Distributed Loads

g	=	gravitational acceleration
m	=	wing mass density per unit span
m_x, m_s, m_n	=	moments about x axis, local spanwise axis, wing-normal axis
p_x, p_s, p_n	=	loads along x axis, local spanwise axis, wing-normal axis

I. Introduction

A STANDARD practice in the calculation of wing aerodynamic forces and resulting structural loads involves decoupling the two problems. Some geometry is assumed, typically corresponding to the unloaded wing or some simple assumed deflection mode, and this geometry is then used for aerodynamic force calculations. This is a very effective approach for moderate to low-aspect ratios, where the deflections are small and hence have little effect on the aerodynamics. A substantial improvement in accuracy over the decoupled procedure can be obtained by incorporating linearized structural deflections into a linear aerodynamic solution and vice versa via influence coefficients. Examples of this technique are given by Caap and Elmeland[1] for a compact fighter configuration and by Grossman et al[2] for a transport wing. For very high aspect ratios, however, large-deflection nonlinear structural theory may be required for sufficient accuracy, especially at limit loads where prediction accuracy is most important. Typical examples are high-performance sailplanes, human powered aircraft, and ultralight high-altitude long-endurance aircraft. If external bracing at small angles to the wing axis is

Received June 10, 1989; presented as Paper 89-2166 at the AIAA 7th Applied Aerodynamics Conference, Seattle, WA, July 31–Aug. 2, 1989; revision received Jan. 25, 1990.

*Carl Richard Soderberg Assistant Professor, Department of Aeronautics and Astronautics. Member AIAA.

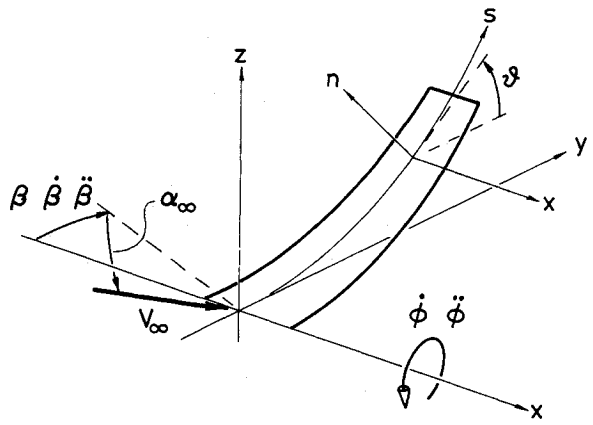

Fig. 1 Coordinates and freestream rotation angles.

employed, nonlinear effects can become especially important in load prediction. The *Daedalus* wing is one example where nonlinear effects dominate near limit-load conditions.

A further complication that arises from large structural deflections is that the applied aerodynamic loads are altered nonlinearly. Indeed, in the *Daedalus*, the nonlinear interaction between the static deflection and sideslip is relied on as the sole roll control mechanism! The brute-force approach to solving such a problem would involve iterating repeatedly between the aerodynamic and structural calculations until the overall structural-aerodynamic solution converges. This tends to be an expensive procedure that is not always guaranteed to converge, especially if the structure is near buckling (as in an externally braced wing). Under-relaxation may be required, which further slows the convergence.

This paper presents a robust and economical procedure for solving the aerodynamic and nonlinear structural problems as a fully coupled system for a high-aspect ratio wing. Lifting line theory governs the spanwise aerodynamic force distributions, and nonlinear bending/torsion beam theory is used to govern the structural response. The structural formulation is assumed static except for rigid-body accelerations. The resulting overall problem for the aerodynamic and structural unknowns is nonlinear, but can be readily solved by a global Newton method. Examples are drawn from the *Daedalus* human powered aircraft wing.

II. Structural Formulation

A system of Cartesian coordinates x, y, z is fixed to the aircraft as shown in Fig. 1. For a high-aspect-ratio wing with large deflections, modeling the wing as a nonlinear beam is very accurate. In most actual applications such as the *Daedalus* wing, only the vertical displacements need to be treated nonlinearly, however. It is therefore appropriate to define a local x-, s-, n-coordinate system attached to the wing that undergoes a simple rotation from the Cartesian x, y, z frame by a simple rotation ϑ about the x axis (Fig. 1).

Figure 2 shows the sign conventions for the structural displacements u, w of the wing reference axis in the Cartesian frame. With the simplifications used in the present formulation, the extensional displacement v does not enter the governing equations and will be neglected. The wing reference axis is defined to lie at the shear center location $(x/c)_{sc}$ of each spanwise station. The torsional twist angle t is defined about this reference axis.

The fully nonlinear beam equations as given in Rivello[3] are suitably simplified by assuming the twist angle t and the fore-aft wing bending deflection u to be small. Only the wing up-down bending deflection w is assumed to be large enough to require nonlinear structural analysis. The deflection angles ϑ and φ are related to the deflections u and w as follows

$$\sin\varphi = (du/ds) \tag{1}$$

$$\sin\vartheta = (dw/ds) \tag{2}$$

Because even small twist angles can have a significant effect on the aerodynamic loading, torsion effects must be included in the overall analysis. These are generally small enough, however, to permit small-angle simplifications. Similarly, fore-aft deflections can have a substantial effect on the pitching moments of the entire wing as well as affecting the torsion indirectly and, hence, must be retained even if they are very small. Relation (1) could therefore be safely approximated as $\varphi = du/ds$ although this would not produce a significant computational advantage.

With the wing modeled as an isotropic slender beam, only the local bending stiffnesses $EI_{xx}, EI_{xn}, EI_{nn}$ and the torsional stiffness GJ are needed for a full structural description of the wing. These are defined in the local rotated wing coordinates x, s, n, as are the tension load P, shear loads S, bending moments M, and torsion T.

The beam equilibrium equations in their nonlinear form are given by Rivello[3]

$$\left(\frac{dP}{ds}\right) + S_x\left(\frac{d\varphi}{ds}\right) + S_n\left(\frac{d\vartheta}{ds}\right) + p_s = 0 \tag{3}$$

$$\left(\frac{dS_x}{ds}\right) - P\left(\frac{d\varphi}{ds}\right) + S_n\left(\frac{dt}{ds}\right) - p_x = 0 \tag{4}$$

$$\left(\frac{dS_n}{ds}\right) - P\left(\frac{d\vartheta}{ds}\right) - S_x\left(\frac{dt}{ds}\right) - p_n = 0 \tag{5}$$

$$\left(\frac{dM_x}{ds}\right) - M_n\left(\frac{dt}{ds}\right) + T\left(\frac{d\varphi}{ds}\right) - S_n + m_x = 0 \tag{6}$$

$$\left(\frac{dM_n}{ds}\right) + M_x\left(\frac{dt}{ds}\right) - T\left(\frac{d\vartheta}{ds}\right) - S_x + m_n = 0 \tag{7}$$

$$\left(\frac{dT}{ds}\right) - M_x\left(\frac{d\varphi}{ds}\right) + M_n\left(\frac{d\vartheta}{ds}\right) + m_s = 0 \tag{8}$$

The standard slender beam stress-deflection relations are used to close the equation system, with φ_0, ϑ_0, t_0, denoting the zero-load (built-in) deflection angles

$$M_x = EI_{xn}\left(\frac{d}{ds}\right)(\varphi - \varphi_0) + EI_{xx}\left(\frac{d}{ds}\right)(\vartheta - \vartheta_0) \tag{9}$$

$$M_n = EI_{nm}\left(\frac{d}{ds}\right)(\varphi - \varphi_0) + EI_{xn}\left(\frac{d}{ds}\right)(\vartheta - \vartheta_0) \tag{10}$$

$$T = GJ\left(\frac{d}{ds}\right)(t - t_0) \tag{11}$$

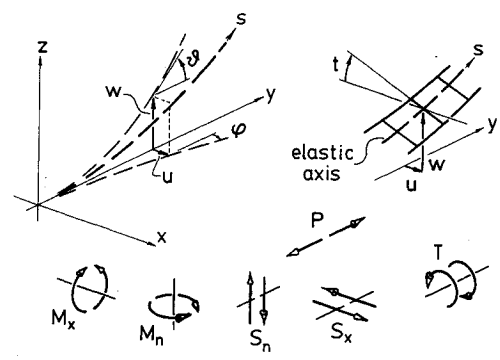

Fig. 2 Displacements and structural loads.

The local section bending stiffnesses EI_{xx}, EI_{xn}, and EI_{nn} are obtained from the specified in-plane and out-of-plane stiffnesses EI_{in}, EI_{out}. For convenience, these are assumed to be defined in the wing's principal bending axes in which the cross-product stiffness vanishes. The principal axes in the unloaded condition are set at the known angle $\bar{t}$ to the x-y plane. In the *Daedalus* wing, a forward main spar is the only significant torsion and out-of-plane bending member. A small rear spar supplies in-plane bending stiffness only. For this case, the in-plane principal axis goes through both spar centers, and the shear center is located at the main spar as shown in Fig. 3. Accounting for the structural twist t, the resulting stiffnesses in the s-n frame are given by the following relations

$$EI_{xx} = EI_{in} \sin^2(\bar{t} + t) + EI_{out} \cos^2(\bar{t} + t) \tag{12}$$

$$EI_{xn} = (EI_{out} - EI_{in}) \sin(\bar{t} + t) \cos(\bar{t} + t) \tag{13}$$

$$EI_{nn} = EI_{in} \cos^2(\bar{t} + t) + EI_{out} \sin^2(\bar{t} + t) \tag{14}$$

The force loading functions p_x, p_s, p_n and moment loading functions m_x, m_s, m_n arise from distributed wing weight, inertial reactions, aerodynamic forces, and external point loads. Examples of point loads are those due to a fuselage, external stores, or external bracing struts or wires. The *Daedalus* wing employs one lift wire with an angle of $\bar{\vartheta}$ attached at $s = s_w$ (approximately the midspan). This exerts a force F_w at a point having a small normal offset Δn_w from the spar neutral plane as illustrated in Fig. 4. The force is applied directly under the shear center (spar position) so that no applied moment about the s axis results, but the offset Δn_w causes an applied moment about the x axis. The fuselage weight exerts a central point load F_f at $s = 0$. The aerodynamic lift forces are assumed to act at the quarter-chord location and normal to the wing's axis and the local relative airflow, with the profile pitching moment coefficient assumed to be constant. The drag forces are taken to act along the relative airflow, whose direction is altered from that of the freestream by the induced downwash angle α_i and roll rate $\dot{\phi}$, which accounts for induced drag and roll-yaw coupling. Both angle corrections are assumed small. The local airspeed is altered from the centerline airspeed via the yaw rate $\dot{\beta}$.

The loading functions for the *Daedalus* wing example are given below, with the point loads represented with the unit impulse function δ

$$p_x = m\ddot{\beta}s + (1/2)\rho V^2 c\, c_d + \rho[\dot{\phi}s + V(\alpha_i - \alpha_\infty \cos\vartheta)]\Gamma \tag{15}$$

$$p_n = F_w \sin(\bar{\vartheta} - \vartheta)\,\delta(s - s_w) - mg\cos\vartheta - F_f\delta(s) - [m + \rho(\pi/4)c^2]\ddot{\phi}s + \rho V\Gamma \tag{16}$$

$$p_s = F_w \cos(\bar{\vartheta} - \vartheta)\delta(s - s_w) - mg\sin\vartheta \tag{17}$$

$$m_x = F_w \cos(\bar{\vartheta} - \vartheta)\delta(s - s_w)\Delta n_w \tag{18}$$

$$m_n = 0 \tag{19}$$

$$m_s = (1/2)\rho V^2 c^2 c_m + \rho V\Gamma c\,[(x/c)_{sc} - (1/4)] \tag{20}$$

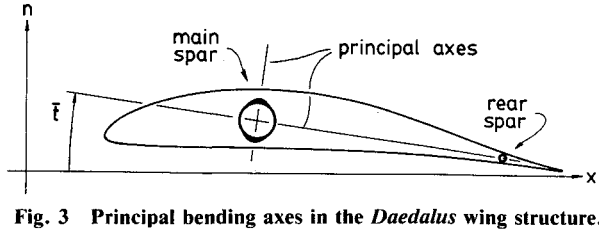

Fig. 3 Principal bending axes in the *Daedalus* wing structure.

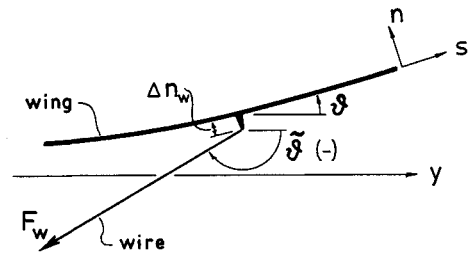

Fig. 4 *Daedalus* wing external wire bracing geometry.

In the case of the *Daedalus* wing, the loading functions involve the lift wire tension F_w. The angle $\bar{\vartheta}$ of the lift wire in the y-z plane is related to the overall geometry and the wing displacements $w(s_w)$ at the wire attach points (see Fig. 4)

$$\cos\bar{\vartheta} = (s_w/\sqrt{[h_w + w(s_w)]^2 + s_w^2}) \tag{21}$$

The lift wire tension is proportional to its strain, which arises directly from the wing displacement at the two lift wire attach points, and can, therefore, be expressed in terms of the local deflection $w(s_w)$ by the following stress-strain relation

$$F^w = EA_w \left\{ \frac{\sqrt{[h_w + w(s_w)]^2 + s_w^2}}{\sqrt{h_w^2 + s_w^2}} - 1 \right\} \tag{22}$$

With a first-order system of 11 equations, 11 boundary conditions must be imposed to obtain a unique solution. For computational symmetry, however, it is better to treat the two wing halves as two coupled structural problems. A total of 22 boundary conditions and compatibility conditions between the two halves are then imposed. At each wingtip ($s = \pm b/2$), zero shear, axial tension, bending moment, and torsion are specified:

$$P(-b/2) = 0, \qquad P(b/2) = 0 \tag{23a}$$

$$S_x(-b/2) = 0, \qquad S_x(b/2) = 0 \tag{23b}$$

$$S_n(-b/2) = 0, \qquad S_n(b/2) = 0 \tag{23c}$$

$$M_x(-b/2) = 0, \qquad M_x(b/2) = 0 \tag{23d}$$

$$M_n(-b/2) = 0, \qquad M_n(b/2) = 0 \tag{23e}$$

$$T(-b/2) = 0, \qquad T(b/2) = 0 \tag{23f}$$

At the wing center, deflections, deflection angles, and twist angles are specified for each wing half

$$u(-0) = 0, \qquad u(+0) = 0 \tag{24a}$$

$$w(-0) = 0, \qquad w(+0) = 0 \tag{24b}$$

$$\varphi(-0) = \varphi_0(-0), \qquad \varphi(+0) = \varphi_0(+0) \tag{24c}$$

$$\vartheta(-0) = \vartheta_0(-0), \qquad \vartheta(+0) = \vartheta_0(+0) \tag{24d}$$

$$t(-0) = t_0(-0), \qquad t(+0) = t_0(+0) \tag{24e}$$

These conditions ensure compatibility between the two wing halves at the centerline. Also, the center point load F_f in Eq. (16), assumed to be applied at $s = 0$, no longer enters the formulation explicitly. The preceding conditions assume that

the wingroot is clamped. The *Daedalus* wing mount is rather unique in that it is pinned in roll and, hence, can transmit no significant rolling moments into the wing. For this special case, the two constraints on $\vartheta(\pm 0)$ must therefore be replaced by conditions of slope and moment continuity

$$\vartheta(-0) - \vartheta(+0) = \vartheta_0(-0) - \vartheta_0(+0) \tag{25}$$

$$M_x(-0) - M_x(+0) = 0 \tag{26}$$

III. Aerodynamic Formulation

A lifting-line formulation with yaw and roll rate effects is used as the aerodynamic model of the wing. The net effective local angle of attack (defined from the zero-lift line) is modified from its built-in value of α by the freestream angle α_∞, induced and α_i, structural twist t, roll rate $\dot{\phi}$, and the coupling between sideslip β and local dihedral angle ϑ. The local circulation Γ is the given by

$$\Gamma = (Vc/2)c_l = (Vc/2)a_0\,[\alpha + \alpha_\infty \cos\vartheta - \alpha_i + t + \vartheta \sin\beta - (\dot{\phi}s/V)] \tag{27}$$

where the local upwash velocity due to roll rate has been approximated by $\dot{\phi}$ in lieu of the exact form $\dot{\phi}\sqrt{(y+v)^2 + w^2}$.

It is still necessary to relate the local α_i in Eq. (27) to the global Γ distribution to obtain a closed system. Here, this is efficiently done by assuming a flat wing and employing standard lifting-line theory. This assumption will have a relatively minor effect on the overall solution because the local aerodynamic lift force will still be properly applied normal to the deflected wing. More exact aerodynamic formulations for α_i (such as vortex lattice) could be incorporated to account properly for extremely large deflections, but at considerably greater computational effort.

In the application of lifting-line wing theory, the spanwise coordinate s is replaced by the spanwise Glauert coordinate θ, with $s = (b/2)\cos\theta$. This coordinate permits an efficient discretization of the circulation Γ as a Fourier series

$$\Gamma(\theta) = \sum_{n=1}^{\infty} A_n \sin n\theta \tag{28}$$

The induced angle corresponding to the associated trailing vorticity is then given by

$$\alpha_i(\theta) = \frac{1}{2Vb}\sum_{n=1}^{\infty} nA_n \frac{\sin n\theta}{\sin\theta} \tag{29}$$

where V is the local air velocity, which can have a spanwise variation due to yaw rate.

$$V(\theta) = V_\infty + \dot{\beta}\,(b/2)\cos\theta \tag{30}$$

In terms of the Fourier coefficients, Eq. (27) becomes the following

$$\sum_{n=1}^{\infty} A_n \left(\sin\theta + n\frac{ca_0}{4b}\right)\sin n\theta = V(ca_0/2)\,[\alpha + \alpha_\infty\cos\vartheta + t + \vartheta\sin\beta - (\dot{\phi}s/V)]\sin\theta \tag{31}$$

For computational purposes, the infinite series in Eq. (31) can be safely truncated to as few as 10 terms for most cases, with more terms being required if aileron or flap deflections are present. If only N terms are retained, N independent equations for the Fourier coefficients A_n ($n = 1,2,\ldots,N$) are obtained through a Fourier decomposition.

$$\int_0^\pi \{\text{Eq. (31)}\}\sin\theta\,d\theta$$

$$\int_0^\pi \{\text{Eq. (31)}\}\sin 2\theta\,d\theta$$

$$\vdots$$

$$\int_0^\pi \{\text{Eq. (31)}\}\sin N\theta\,d\theta \tag{32}$$

These equations depend on the structural twist t and deflection angle ϑ; hence, the Fourier coefficients are coupled to the structural solution as well as the aircraft angle of attack α_∞, sideslip β, and roll rate $\dot{\phi}$. None of these quantities are known a priori in the general case where, for example, only the overall lift or rolling moment and/or yawing moment may be known or prescribed. Hence, α, β, and $\dot{\phi}$ require additional constraints to fix them. These are readily obtained as appropriately weighted spanwise integrals of the aerodynamic, gravitational, and inertial forces

$$\mathfrak{L} = \int_{-b/2}^{b/2} [-mg + \rho V\Gamma\cos\vartheta]\,ds \tag{33}$$

$$\mathfrak{M} = \int_{-b/2}^{b/2} [-m\ddot{\phi}s + \rho V\Gamma]\,s\,ds \tag{34}$$

$$\mathfrak{N} = \int_{-b/2}^{b/2} \left[m\ddot{\beta}s + \frac{\rho V^2}{2}c_d + \rho(V\alpha_i - \dot{\phi}s)\Gamma\right] s\,ds \tag{35}$$

The moment definitions [Eqs. (34) and (35)] use the spanwise arc length coordinate s as the moment arm for the forces at that spanwise location. This is an approximation made for computational simplicity. The associated errors are negligible because precise knowledge of the overall roll and yaw moments is not very important for accurate structural load predictions. The lift can be very important, however, and in Eq. (33) force components are accounted for to second order in the wing deflection. Note that the rolling moment definition [Eqs (34)] includes the inertial reaction from the roll acceleration $\ddot{\phi}$, so that $\mathfrak{M}$, as defined, will invariably be zero in actual applications (assuming, of course, that the wing accelerates in roll as a rigid body, necessary with a static load theory). Extenal yaw moments can be applied at the wing root with the rudder, however, meaning that $\mathfrak{N}$ will not necessarily be zero. The moment definitions [Eqs. (34) and (35)] assume that the wing is symmetric in mass distribution. Accounting for nonsymmetry would result in only minor complications.

IV. Coupled System Solution

The structural problem to be solved is defined by the two displacement-angle relations [Eqs. (1) and (2)], the six equilibrium equations [Eqs. (3–8)], and the three stress-deflection relations [Eqs. (9–11)]. These constitute a first-order system of 11 equations in the 11 unknowns u, w, φ, ϑ, t, P, S_x, S_n, M_x, M_n, T. These unknowns are local in the sense that they are functions of the spanwise coordinate s. The first-order system also depends on global unknowns, which appear in the loading functions defined by Eqs. (15–20). These are the circulation Fourier coefficients A_1, A_2,...A_N and the global operating parameters α_∞, β, $\dot{\beta}$, $\ddot{\beta}$, $\dot{\phi}$, $\ddot{\phi}$. The N Fourier coefficients are constrained by N equations [Eqs. (32)]. The applied forces are either specified or related to the attachment point displacements as in Eq. (22). The operating parameters are either specified or implicitly defined by enforcing any number of the three lift and moment relations [Eqs. (33–35)].

A. Discretization

The structural problem is discretized using the well-known Keller box finite-difference scheme,[4] which is second-order accurate for arbitrary grid node distributions. The wing is divided into a suitable number of spanwise stations (or grid nodes) at $\theta = \theta_j$, with j being the spanwise index ($-J \le j \le J$). An ideal distribution for resolving the steep circulation gradients near the wingtips is a uniform node spacing in θ, which produces a cosine spacing in the physical spanwise coordinate s. The structural solution, however, dictates a more or less uniform discretization in s. An effective compromise is struck with the following distribution formula for θ_j

$$\theta_j = (\pi/2)\,\{1 - (1/2)\,(j/J)\,[1 + (|j|/J)]\} \tag{36}$$

$$s_j = (b/2)\cos\theta_j \tag{37}$$

For a given total number of nodes $2J$, this results in node spacing at the wing center being reduced by a factor of 1/2 from the pure cosine spacing. The tip spacing is increased by a factor of 3/2 but still properly resolves the circulation gradient.

The node distribution defined by Eq. (36) is modified slightly to ensure that a node falls wherever a point load is applied. In the case of the *Daedalus* wing, this corresponds to the station where the lift wire is attached. This index of this node is denoted by j_w so that $s_{j_w} = s_w$. Also, the $j_w + 1$ node is placed at the same location, so that $s_{j_w+1} - s_{j_w} = 0$ (see Fig. 5). This zero-width interval permits the lift wire load to be introduced as a perfect discontinuity in the shear (for example), with no significant modifications to the finite difference formulas. Likewise, the $j = -1,0,1$ nodes all coincide at the centerline to allow for the fuselage load.

The Keller box differencing scheme applied to the first-order structural system results in 11 finite-difference equations at each $(j, j+1)$ interval. For example, Eq. (1) is discretized as

$$\Delta s_{j+1/2} \sin\,[(\varphi_{j+1} + \varphi_j/2)] - u_{j+1} + u_j \equiv R_{uj} = 0 \tag{38}$$

where

$$\Delta s_{j+1/2} = s_{j+1} - s_j$$

Note that at the zero-width $(j_w, j_w + 1)$ interval for which $\Delta s = 0$ the above equation automatically assumes the correct u-displacement continuity form

$$-u_{j+1} + u_j = 0 \tag{39}$$

with no special treatment.

Equation (5), after being combined with the distributed normal load definition [Eq. (16)], is discretized as follows

$$S_{nj+1} - S_{nj} - \frac{P_{j+1} + P_j}{2}(\varphi_{j+1} - \varphi_j) + \frac{S_{xj+1} + S_{xj}}{2}(t_{j+1} - t_j)$$

$$- \Delta s_{j+1/2}\,\rho\left(V_\infty + \dot\phi\,\frac{s_{j+1} + s_j}{2}\right)\sum_n A_n \sin n\theta$$

$$- \Delta s_{j+1/2}\,\frac{m_{j+1} + m_j}{2} g \sin\left(\frac{\vartheta_{j+1} + \vartheta_j}{2}\right)$$

$$+ F_w \sin\left(\tilde\vartheta - \frac{\vartheta_{j+1} + \vartheta_j}{2}\right)\delta_{j,j_w} \equiv R_{s_j} = 0 \tag{40}$$

In Eq. (40), the wire angle $\tilde\vartheta$ and tension F_w are defined in terms of ϑ_{j_w} by Eqs. (21) and (22). Also, the product $\Delta s\,\delta(s - s_w)$ has been replaced by the Kronecker delta δ_{j,j_w}. Note that for the zero-width $(j_w, j_w + 1)$ interval where the lift wire

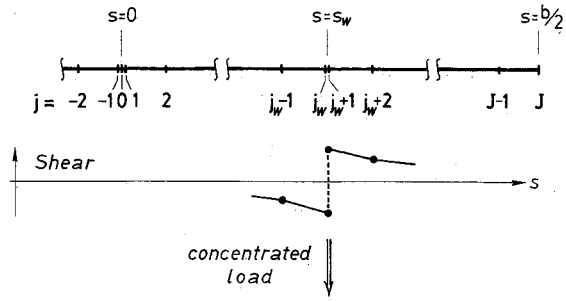

Fig. 5 Node indexing and admitted solution discontinuity.

is attached Eq. (40) automatically reverts to

$$S_{nj+1} - S_{nj} = -F_w \sin\,(\tilde\vartheta - \vartheta_{j_w}) \tag{41}$$

which gives the correct jump in the shear S_n due to the normal lift wire load component. Again, no special differencing form is required at this interval.

Eq. (32), which constrain the Fourier circulation coefficients, is put into discrete form by simple trapezoidal summation

$$\sum_{j=-J}^{J-1} \sin\theta_{j+1/2}\Delta\theta_{j+1/2}$$

$$\left\{\sum_n A_n \left(\sin\theta + n\frac{ca_o}{4b}\right)_{j+1/2} \sin n\theta_{j+1/2}\right.$$

$$\left. - \left[V\frac{ca_o}{2}\left(\alpha + \alpha_\infty \cos\varphi + t + \vartheta \sin\beta - \frac{s\dot\phi}{V}\right)\sin\theta\right]_{j+1/2}\right\}$$

$$\equiv R_{An} = 0 \tag{42}$$

where the subscript $j + 1/2$ implies a simple average between $j + 1$ and j.

B. Newton System

The nonlinear system to be solved has the form

$$\boldsymbol{R}(\boldsymbol{U}) = 0 \tag{43}$$

where $\boldsymbol{U}$ is the unknown vector whose components consist of all the local structural unknowns and global aerodynamic unknowns. $\boldsymbol{R}$ is a vector function whose components consist of local finite-difference residual functions such as R_{uj}, R_{Sj}, as defined by Eqs. (38) and (40), or discretized global constraint residuals such as R_{An}, as defined by Eq. (42). Given an approximate solution $\boldsymbol{U}^\nu$ at iteration level ν, the change $\delta\boldsymbol{U}$ needed to obtain an improved guess $\boldsymbol{U}^{\nu+1}$ is determined by solving exactly the linearized form of Eq. (43)

$$\left[\frac{\partial \boldsymbol{R}}{\partial \boldsymbol{U}}\right]^\nu \delta\boldsymbol{U} = -\boldsymbol{R}^\nu \tag{44}$$

$$\boldsymbol{U}^{\nu+1} = \boldsymbol{U}^\nu + \delta\boldsymbol{U} \tag{45}$$

which drives the residual vector $\boldsymbol{R}$ closer to zero. The known Jacobian matrix $\partial\boldsymbol{R}/\partial\boldsymbol{U}$ in Eq. (44) consists of a block tridiagonal matrix with $2J$ rows of 11×11 blocks filled with partial derivatives of the structural residual functions such as Eq. (40)

$$R_{Sj}\,(\varphi_j, \vartheta_j, t_j, P_j, S_{xj}, S_{nj},$$

$$\varphi_{j+1}, \vartheta_{j+1}, t_{j+1}, P_{j+1}, S_{xj+1}, S_{nj+1}, A_1, A_2, \ldots A_N, \dot\phi)$$

evaluated with the current approximate solution. Each block row also contains a number of full columns corresponding to the global variables because R_{Sj} also depends on the global variables $A_1, A_2, \ldots A_N, \phi$.. The Jacobian matrix also contains

an additional small number of rows (one for each global variable) corresponding to the linearized global constraint functions such as

$$R_{An}(\vartheta_{-J}, t_{-J}, \vartheta_{-J+1}, t_{-J+1}, \ldots, \vartheta_J, t_J, A_1, A_2, \ldots, A_N, \alpha_\infty, \beta, \dot{\beta}, \dot{\phi})$$

which is given fully by Eq. (32). However, since R_{An} depends on structural variables at all spanwise stations, these rows are generally full. This precludes solving the linear Newton system [Eq. (44)] by a standard block-elimination algorithm. To simplify the overall solution procedure, the Newton system is split into two systems—a large, sparse, strictly block-triagonal system for the changes in the local structural unknowns δU_l and a relatively small, generally full system for the changes in the global aerodynamic unknowns and operating parameters δU_g.

$$\left[\frac{\partial R_l}{\partial U_l}\right]^\nu \delta U_l = -R_l^\nu - \left[\frac{\partial R_l}{\partial U_g}\right]^\nu \delta U_g \tag{46}$$

$$\left[\frac{\partial R_g}{\partial U_g}\right]^\nu \delta U_g = -R_g^\nu - \left[\frac{\partial R_g}{\partial U_l}\right]^\nu \delta U_l \tag{47}$$

Equation (46) with the multiple right-hand sides is readily solved by a standard block elimination method to give

$$\delta U_l = -r - [\bar{s}]\,\delta U_g \tag{48}$$

which is substituted into Eq. (47) to produce

$$\left[\left(\frac{\partial R_g}{\partial U_g}\right) - \left(\frac{\partial R_g}{\partial U_l}\right) s\right]^\nu \delta U_g = -R_g^\nu + \left(\frac{\partial R_g}{\partial U_l}\right)^\nu r \tag{49}$$

which is a full but relatively small system involving only the global variable changes δU_g as unknowns and is easily solved by the Gaussian elimination. By substituting δU_g back into the partially determined system [Eq. (48)], the local variable changes δU_l are completely determined. The local and global solution can now be updated,

$$U_l^{\nu+1} = U_l^\nu + \delta U_l, \qquad U_g^{\nu+1} = U_g^\nu + \delta U_g \tag{50}$$

and the overall process repeated if the changes are above a convergence tolerance. For the *Daedalus* wing in level flight conditions, about three Newton iterations are required to converge to machine accuracy. If the solution is close to a structural instability, however, as many as eight iterations may be required.

V. Validation and Applications

The complexity and degree of generality of the present method makes thorough validation of the theoretical formulation and the computational implementation quite difficult. Limiting problems for which analytic solutions are available

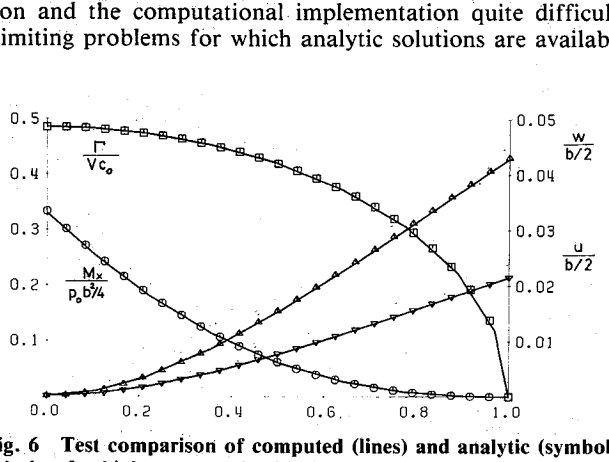

Fig. 6 Test comparison of computed (lines) and analytic (symbols) solution for high-aspect ratio elliptical wing.

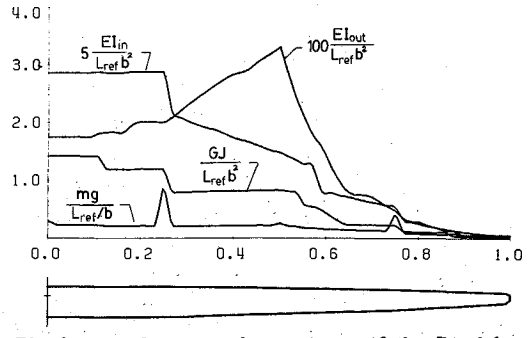

Fig. 7 Planform and structural parameters of the *Daedalus* wing; L_{ref} = 230 lb, b = 112 ft.

can be calculated to validate the bulk of the implementation. A further test of the overall coupled structural/aerodynamic formulation results from comparisons with structural measurements of the *Daedalus* wing under load.

A. Elliptically Loaded Wing

If the following simplifications are made, an analytically tractable aerodynamic/structural problem results:

1) Deflections and structural twists ae made small by specifying EI_{in}, EI_{out}, $GJ \gg \mathcal{L}b^2$, $mg = 0$.

2) The external loads and spar compression are zero $F_w = P = 0$.

3) The wing has no twist (α = constant) and has an elliptical planform $c = c_o \sin\theta$.

4) Yaw and roll angles, rates, and accelerations are zero $\beta = \dot{\beta} = \ddot{\beta} = 0$, $\phi = \dot{\phi} = \ddot{\phi} = 0$.

5) Nonuniform bending stiffnesses of the form $EI \sim \sin\theta$ are chosen (which also tests the representation of a nonuniform beam).

According to classical lifting-line theory, a wing with an elliptic planform and no twist experiences an elliptic spanwise circulation distribution $\Gamma = A_1 \sin\theta$. The first harmonic coefficient is given by

$$A_1 = (1/2)c_o V\{a_o/[(1 + (a_o c_o)/4b)]\}\alpha \tag{51}$$

and all higher harmonics are zero. By specifying a zero wing mass distribution, excluding all point loads and acceleration effects, and assuming negligible induced drag (high-aspect ratio), the only loading function is

$$p_n = \rho V_\infty \dot{A}_1 \sin\theta = p_o \sin\theta \tag{52}$$

for which an analytic solution can be obtained for all the structural variables.

Figure 6 compares the computed circulation distribution Γ, bending moment M_x, and deflections u and w with the analytical solution for a high-aspect ratio ($b/c_o = 100$) elliptical wing for which all the previous assumptions hold. The in-plane and out-of-plane bending stiffnesses were chosen so that $EI_{in} = 3EI_{out}$, and the wing's local principal bending axis angle was specified to be at $\bar{\imath} = 45$ deg to the $x - y$ plane. This tests the implementation of the local stiffness relations [Eqs. (12-14)] and the cross coupling in the moment-deflection relations [Eqs. (9) and (10)]. Despite the relatively small number of points ($J = 11$), the solutions match perfectly. Since the aerodynamic formulation determines the beam loading and the structural formulation determines the resulting structural moments and deflections, both formulations are checked for correctness in this test. The computation time required for this case was 5 s CPU on a Micro Vax II.

B. *Daedalus* Wing — Level Flight

The present calculation method was extensively employed in the wing design for the *Daedalus* human powered aircraft. The

actual planform and structural parameters of this wing are shown in Fig. 7. The parameter discontinuities are due to stepping of the graphite-epoxy plys in the main spar. The wing's overall aspect ratio is 38, making it an ideal application for the present method.

Figure 8 shows the computed loading, shear, and moment distributions on the wing in level flight. A typical airspeed of 22 ft/s and a gross weight of 240 lb were specified for this case, and the corresponding overall angle of attack α_∞ was automatically determined by the global Newton solution scheme. Also shown is a photograph of the aircraft in flight under these operating conditions. The calculated and observed wing deflection shapes agree perfectly to within plotting accuracy. Note that the structural load discontinuities due to the wire and fuselage loads are captured exactly as discussed previously. This calculation was performed with $J = 51$ points on

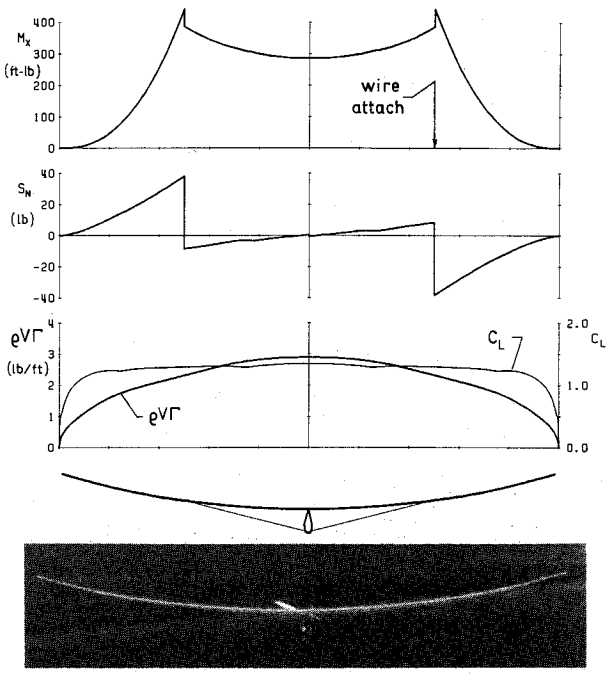

Fig. 8 Calculated structural loads on the *Daedalus* wing in level flight, with photograph of actual aircraft.

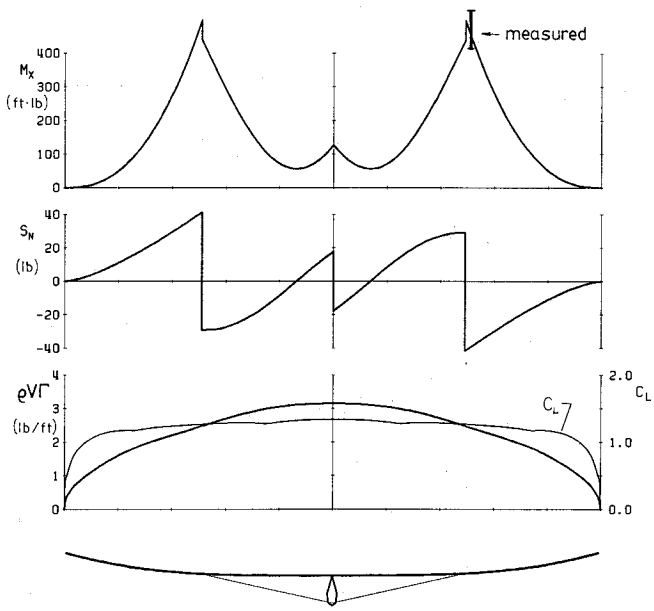

Fig. 9 Calculated structural loads on the *Light Eagle* wing in level flight, with measured bending moment range.

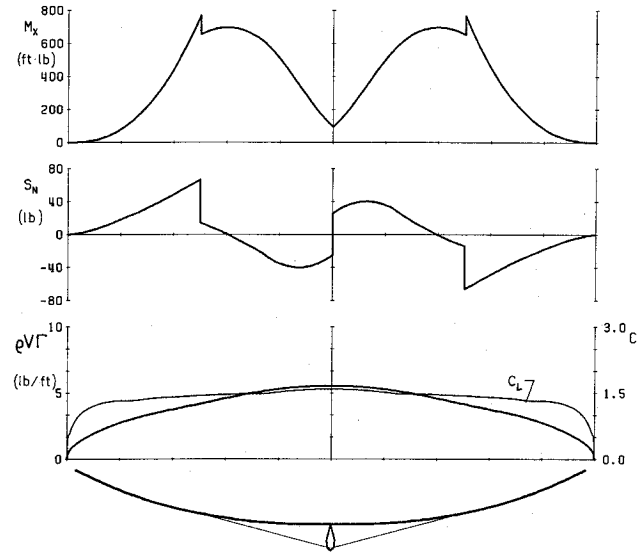

Fig. 10 Calculated structural loads on the *Daedalus* wing in a 1.8-*g* pullup.

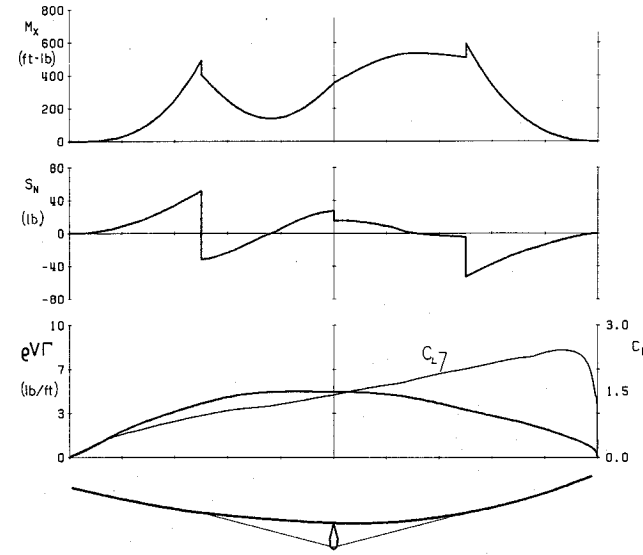

Fig. 11 Calculated structural loads on the *Daedalus* wing in a 1.6-*g* pullup with a 30 deg sideslip angle.

each wing half and $N = 11$ circulation harmonics. Three Newton iterations were required with a total of 60 s CPU time.

In-flight strain gauge measurements were taken on the *Light Eagle* aircraft, which served as a prototype for the *Daedalus*. Figure 9 shows the bending moment distribution with the range of values measured just outboard of the wire attachment points. The strain gauges were calibrated by directly applying known bending moments to the wing in the hangar. A 10 Hz data sampling rate used over a flight period of several minutes gave a large number of quite reliable data points. The spread in the measurements is apparently caused mainly by gust loads. The mean measured moment compares quite well with the calculation.

C. High-lift and Maneuvering Loads

Because of very strong pitch damping and a cruise lift coefficient close to stall, it is nearly impossible to exceed 1.1 *g* on the *Daedalus* with full stick deflections, as the *Light Eagle* flight tests have shown.[5] Nevertheless, the wing must be stressed to higher *g* loads since gusts, higher speeds, and slipping maneuvers greatly aggravate the situation.

The *Daedalus* wing was nominally stressed to 1.8 *g*.[6] A straight-pullup calculation, with the normal level-flight lift

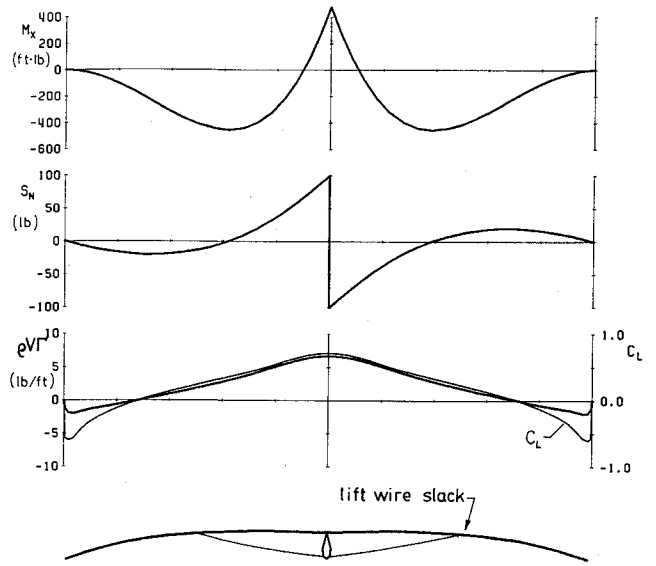

Fig. 12 Calculated structural loads on the *Daedalus* wing near divergence speed.

and the wing mass distribution both multiplied by the 1.8 load factor, is shown in Fig. 10. A relatively high airspeed of 28 ft/s is specified to avoid unrealistically high lift coefficients. The wing is in no danger of buckling, although material stresses are just exceeded in the wing spar.

In Fig. 11, a $\beta = 30$-deg sideslip is combined with a 1.6 g pullup. Such seemingly extreme sideslip angles were actually measured on the *Light Eagle* aircraft, which was equipped with an air data system. This maneuver is representative of a panic recovery from an imminent spiral dive—not an infrequent occurrence in human powered aircraft. The wing has nearly snapped through on the right wing (yawed into the airstream), with the attendant bending moment increases. Specifying a load factor or 1.65 g results in failure of the Newton algorithm to converge, indicating buckling. This shows the dramatic effects on the load margin that can result from unfavorable flight attitude combinations. It must be stressed that the nonlinear fully coupled formulation of the present analysis is essential to capture this behavior and was crucial in the structural design of the *Daedalus* wing for actual flight conditions.

It is important to point out that, in addition to the sideslip β, the calculated loads can be quite sensitive to the particular values of yaw $\dot{\beta}$ and roll rate $\dot{\phi}$ selected. For the preceding case, a zero roll rate $\dot{\phi} = 0$ was specified, and the yaw rate $\dot{\beta}$ was implicitly determined by specifying a zero net rolling moment $\mathfrak{M}$ with Eq. (34). This corresponds to a steady-state turn with the constant sideslip β overcoming the inward rolling moment due to the yaw rate. Equivalently, a zero yaw rate $\dot{\beta}$ could be specified and the roll rate $\dot{\phi}$ determined as a result. This flexibility is very valuable in quickly investigating various flight situations to determine the likeliest failure scenario. For any flight situation, aerodynamic performance values such as induced drag are also determined, allowing the estimation of drag penalties from maneuvering flight.

D. Divergence Speed

The current method is capable of estimating the speed at which structural divergence occurs. Figure 12 shows the structural solution of the *Daedalus* wing for the rather high speed of 45 ft/s. The wing is very serverly twisted due to the airfoil pitching moment, and the wing tips are close to tuck-in. If a flight speed of 48 ft/s is specified, the Newton algorithm refuses to convege, indicating divergence. For this particular aircraft, this divergence sped could only be achieved with an unreasonably steep dive.

A very similar approach could be used to determine aileron erversal speeds. The effect of an aileron is incorporated by a modification of the local aerodynamic angle α and pitching moment coeffieient c_m. By monitoring the net rolling moment on the aircraft, it is a simple matter to determine the reversal airspeed at which the structural twist t over the entire wing caused by the additional aileron pitching moment overcomes the effective addition to α at the aileron location.

IV. Conclusions

A method for the simultaneous calculation of aerodynamic and structural loads has been developed and applied to the design and analysis of a flexible high-aspect ratio wing. The strong coupling between static deflections and aerodynamic loads has been treated by solving the entire nonlinear aerodynamic/structural equation set as a fully coupled system by a global Newton method. The overall scheme is very accurate, robust, and computationally economical.

Calculated examples illustrated the versatility of this numerical tool for the prediction of structural loads for design and limit loads and the determination of lateral stability derivatives and aerodynamic performance in the presence of large static deflections. Flight modes that include any combination of roll and yaw angles, angle rates, and angular accelerations can also be simulated to determine loads and aerodynamic performance under these conditions.

Although the present method is applicable to any moderate to high-aspect ratio wing, it is especially valuable in relatively flexible aircraft. Applications for which the present method is particularly well-suited include human powered aircraft, very high-altitude remotely piloted vehicles, and high-performance sailplanes.

Acknowledgments

This research was supported by the Massachusetts Institute of Technology Dean of Engineering Office.

References

[1]Caap, P., and Elmeland, L., "Calculation of Static Elastic Effects on a Modern High Performance Fighter Aircraft," AIAA Paper 86-1771, June 1986.

[2]Grossman, B., Hafka, R. T., Kao, P. J., Polen, D. M., Rais-Rohani, M., and Sobieszczanski-Sobieski, J., "Intergrated Aerodynamic-Structural Design of a Transport Wing," AIAA Paper 89-2129, July 1989.

[3]Rivello, R. M. *Theory and Analysis of Flight Structures*, McGraw-Hill, New York, 1969.

[4]Keller, H. B., and Cebeci, T., "Accurate Numerical Methods for Boundary Layer Flows: I. Two Dimensional Laminar Flows," *Lecture Notes in Physics*, Vol. 8, Springer-Verlag, NewYork, 1971, p. 92.

[5]Sullian, R. B., and Zerweckh, S. H., "Flight Test Results for the *Daedulus* and *Light Eagle* Powered Aircraft," MIT Aeronautics and Astronautics Dept., Cambridge, MA, Rept. for NASA Grant MAG-1-836, 1988.

[6]Crus, J. R., "Structural Design Conditions and Load Determination for Human Powered Aircraft," *Technical Soaring* (to be published).